Phase Field Modeling of Cyclic Austenite-Ferrite Transformations in Fe-C-Mn Alloys

Article *in* Metallurgical and Materials Transactions A · June 2016

DOI: 10.1007/s11661-016-3595-3

3 authors:

Hao Chen
Tsinghua University
37 PUBLICATIONS **317** CITATIONS
SEE PROFILE

Benqiang Zhu
University of British Columbia - Vancouver
7 PUBLICATIONS **25** CITATIONS
SEE PROFILE

Matthias Militzer
University of British Columbia - Vancouver
31 PUBLICATIONS **237** CITATIONS
SEE PROFILE

Phase Field Modeling of Cyclic Austenite-Ferrite Transformations in Fe-C-Mn Alloys

HAO CHEN, BENQIANG ZHU, and MATTHIAS MILITZER

Three different approaches for considering the effect of Mn on the austenite-ferrite interface migration in an Fe-0.1C-0.5Mn alloy have been coupled with a phase field model (PFM). In the first approach (PFM-I), only long-range C diffusion is considered while Mn is assumed to be immobile during the phase transformations. Both long-range C and Mn diffusions are considered in the second approach (PFM-II). In the third approach (PFM-III), long-range C diffusion is considered in combination with the Gibbs energy dissipation due to Mn diffusion inside the interface instead of solving for long-range diffusion of Mn. The three PFM approaches are first benchmarked with isothermal austenite-to-ferrite transformation at 1058.15 K (785 °C) before considering cyclic phase transformations. It is found that PFM-II can predict the stagnant stage and growth retardation experimentally observed during cycling transformations, whereas PFM-III can only replicate the stagnant stage but not the growth retardation and PFM-I predicts neither the stagnant stage nor the growth retardation. The results of this study suggest a significant role of Mn redistribution near the interface on reducing transformation rates, which should, therefore, be considered in future simulations of austenite-ferrite transformations in steels, particularly at temperatures in the intercritical range and above.

DOI: 10.1007/s11661-016-3595-3

I. INTRODUCTION

PHASE transformations in steels have been studied for more than a century due to their practical importance in steel design and production, and various aspects of these phase transformations were discussed thoroughly in the literature.[1–3] Recently, the specific topic of alloying element effects on migrating interfaces (ALEMI) in steels has attracted significant attention from the phase transformation community, and much effort has been made to improve the understanding of this topic.[4,5] Two classical models, *i.e.*, paraequilibrium (PE)[6,7] and local equilibrium (LE),[8–10] have been proposed to describe the interface condition during the austenite-ferrite transformation in Fe-C-X alloys, where X is a substitutional alloying element, *e.g.*, Mn, Cr, Ni, or Mo. PE is a constrained equilibrium where it is assumed that the chemical potential of C is constant across the interface while there is no redistribution of X during the phase transformation in Fe-C-X alloys. Therefore, the PE model predicts that the transformation is purely controlled by carbon diffusion. On the other hand, the LE model adopts full local equilibrium, in which the chemical potential of both C and X is assumed to be constant across the interface. Based on this assumption, the transformation rate is determined either by C diffusion or X diffusion. Due to the large difference in diffusivities of C and X, there are two different partitioning modes of X during the phase transformations. In the first mode, the kinetics of interface migration is controlled by carbon diffusion, and the concentration of X in the growing phase is the same as that in the parent phase. However, due to LE conditions, a "spike" of X is moving ahead of the interface. This mode has been termed "local equilibrium with negligible partitioning" (LE-NP). In the second mode, the carbon concentration gradient in the parent phase is almost negligible while that of X is large. Hence, the transformation rate is slow and controlled by diffusion of X. This mode has been termed "local equilibrium with partitioning" (LE-P). In order to explore the transition among PE, LE-NP, and LE-P, several phenomenological models have been developed[11–16] where also the effect of X segregation at the interface on transformation kinetics is taken into account using Cahn's solute drag[17] or Hillert's Gibbs energy dissipation theory,[18] respectively. The solute drag theory suggests that the segregation of X leads to a drag pressure on the migrating interface, and the magnitude of the drag pressure depends on the interface velocity. According to the Gibbs energy dissipation theory, the trans-interface diffusion of X causes dissipation of Gibbs energy, the magnitude of which is also affected by the interface velocity. Comparing these two approach shows that they are equivalent,[19,20] *i.e.*, the solute drag pressure is equal to Gibbs energy

HAO CHEN, Assistant professor, is with the Key Laboratory for Advanced Materials of Ministry of Education, School of Materials Science and Engineering, Tsinghua University, Beijing, China. Contact e-mail: hao.chen@mail.tsinghua.edu.cn BENQIANG ZHU, Ph.D. Student, and MATTHIAS MILITZER, Professor, are with the Centre for Metallurgical Process Engineering, The University of British Columbia, Vancouver, V6T 1Z4, Canada.
Manuscript submitted December 11, 2015.

Published online: 09 June 2016

dissipation. For consistency, the term "Gibbs energy dissipation" will be used in the present work.

A number of dedicated experiments have been performed to investigate alloying element effects on migrating austenite-ferrite interfaces, *e.g.*, conventional isothermal or continuous heating/cooling experiments,[21–24] decarburization experiments,[25–27] gradient experiments,[28] and cyclic phase transformation experiments.[29–31] In particular, the cyclic phase transformation experiments have been conducted in Fe-C-Mn alloys using dilatometry to investigate the effect of Mn on migrating austenite-ferrite interfaces. The temperature cycle and dilatation response for a type I (immediate) cyclic phase transformation test in an Fe-0.1C-0.5Mn alloy are reproduced in Figures 1(a) and (b). The cycling temperatures were 1058.15 K and 1115.15 K (785 °C and 842 °C). Linear expansion and contraction stages, which are considered as evidence of no phase transformation or an extremely sluggish transformation, have been observed at the beginning of heating and cooling, respectively, and they have been called "stagnant stages."[32] As the nucleation process is not required during the cyclic phase transformation, the stagnant stage is not caused by nucleation incubation. In previous work,[33] it was directly observed by high-temperature laser confocal microscopy that the austenite/ferrite interface is nearly immobile in the stagnant stage during the cyclic phase transformation. During cooling after the cyclic phase transformation, a special growth retardation stage has been identified at around 1058.15 K (785 °C) for the final austenite-to-ferrite transformation,[32] as shown in Figure 1(b).

The cyclic phase transformation experiments in Fe-C-Mn alloys have been used to benchmark sharp interface models assuming diffusion controlled transformation in the limits of LE and PE. It was found that the LE model can qualitatively predict the stagnant stage and growth retardation while the PE model does not capture these two features.[34] This indicates that Mn partitioning at the interface plays a significant role in controlling the cyclic transformation behavior. Considering Mn diffusion in the LE model is, however, numerically expensive. Thus, Gamsjäger *et al.* used a mixed-mode model that combines carbon diffusion with an effective interface mobility,[35] which is numerically efficient. The effect of Mn partitioning on interface migration is taken into account in the effective interface mobility. It is, however, also interesting to use mixed-mode models that account for the role of Mn to describe and further analyze the cyclic phase transformations.

The mixed-mode concept can naturally be incorporated into phase field models which, as a powerful technique of simulating microstructure evolution, have been increasingly applied to simulating the austenite-ferrite transformation in steels.[36–41] Despite its great importance, the effect of alloying elements on migrating austenite/ferrite interfaces has received limited attention from the phase field community. In most phase field simulations, it is assumed that there is only C redistribution while X is immobile during the phase transformations. Thus, an approach is required to evaluate the alloying elements effect on transformation kinetics in phase field modeling. Furthermore, previous phase transformation simulations emphasized binary or quasi-binary alloys, and it is important to extend these simulations to ternary or even higher multi-component systems that are in general more relevant for commercial steels.

In the present work, three different approaches accounting for the effect of Mn on migrating austenite-ferrite interfaces are introduced into a phase field model (PFM), *i.e.*, (i) PFM-I, in which only long-range C diffusion is considered while Mn is assumed to be immobile; (ii) PFM-II, in which both C and Mn long-range diffusion are considered; (iii) PFM-III, in which long-range diffusion of C is considered together with the Gibbs energy dissipation due to Mn diffusion inside the interface. The cyclic austenite-ferrite transformations in the Fe-0.1C-0.5Mn alloy are utilized to evaluate these three models.

II. MODEL

In the current study, a single phase field model will be used to simulate the austenite-ferrite transformation in an Fe-0.1C-0.5Mn alloy. The value of the phase field variable ϕ is equal to 1 for austenite and 0 for ferrite, and changes continuously from 0 to 1 through a diffusive interface with a thickness of η. The temporal evolution of the phase field variable is described by[42,43]

$$\frac{\mathrm{d}\phi}{\mathrm{d}t} = M_{\gamma\alpha}\left\{\sigma_{\gamma\alpha}\left[\nabla^2\phi + \frac{\pi^2}{2\eta^2}(2\phi - 1)\right] + \frac{\pi}{\eta}\sqrt{(1-\phi)\phi}\Delta G_{\gamma\alpha}\right\}. \quad [1]$$

Here $M_{\gamma\alpha}$ is the interface mobility, $\sigma_{\gamma\alpha}$ is the interface energy, and $\Delta G_{\gamma\alpha}$ is the driving pressure.

Diffusion of elements i = C and Mn is coupled to the phase field model, *i.e.*,

$$\frac{\partial X_i}{\partial t} = \nabla\left[D_i^{\gamma}\phi\nabla X_i^{\gamma} + D_i^{\alpha}(1-\phi)\nabla X_i^{\alpha}\right], \quad [2]$$

where D_i^{γ} and D_i^{α} are diffusivities of element i in austenite and ferrite, X_i is the local concentration of i. X_i is the sum of phase concentrations (X_i^{α} and X_i^{γ}) weighted with the phase field parameter:

$$X_i = (1-\phi)X_i^{\alpha} + \phi X_i^{\gamma}. \quad [3]$$

The redistribution of i between austenite and ferrite within the interface is approximated by the equilibrium ratio[39]

$$k_i^{\mathrm{eq}} = \frac{X_i^{\alpha}}{X_i^{\gamma}} = \frac{X_i^{\alpha\text{-eq}}}{X_i^{\gamma\text{-eq}}}, \quad [4]$$

where $X_i^{\alpha\text{-eq}}$ and $X_i^{\gamma\text{-eq}}$ are the equilibrium concentrations of i in ferrite and austenite, respectively.

Three different PFM approaches are evaluated in the present study:

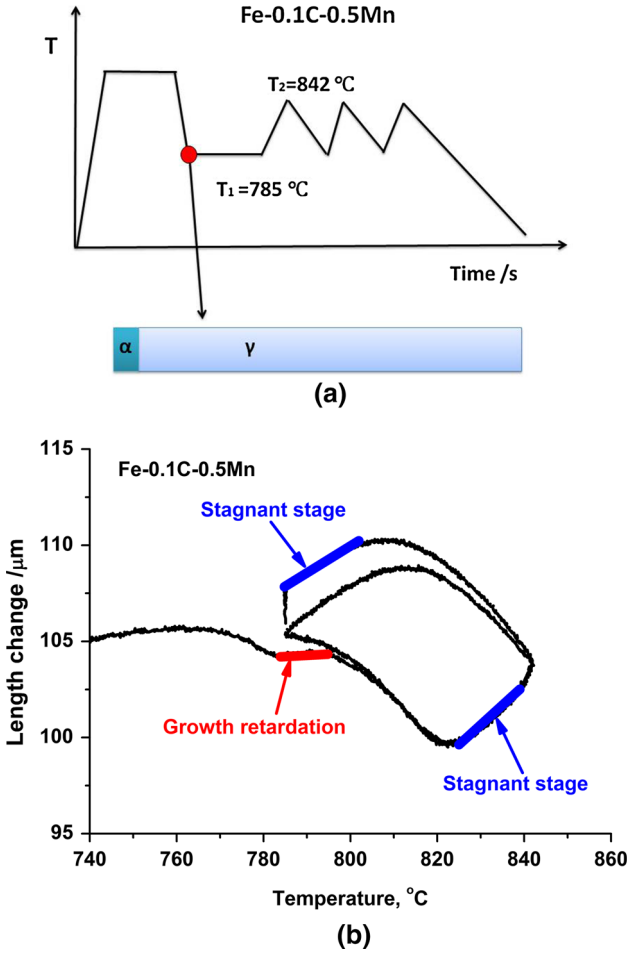

Fig. 1—(*a*) Temperature program for the type I (immediate) cyclic phase transformations in the Fe-0.1C-0.5Mn alloy; (*b*) the dilatation response as a function of temperature during the cyclic phase transformations.[31]

PFM-I In PFM-I, only long-range C diffusion is considered while Mn is assumed to be immobile. The role of interface mobility is taken into account such that PFM-I constitutes a binary mixed-mode model.[44–48]

PFM-II Long-range diffusion of both C and Mn are considered in PFM-II. PFM-II constitutes a mixed-mode model for ternary alloys.

PFM-III In PFM-III, while only long-range carbon diffusion is considered, the Gibbs energy dissipation ΔG^{dis} due to Mn diffusion inside the austenite/ferrite interface is taken into account, *i.e.*,[17,18]

$$\Delta G^{\text{dis}} = \int_{-\Lambda}^{+\Lambda} (X_0 - X(x)) \frac{\mathrm{d}E(x)}{\mathrm{d}x} \mathrm{d}x. \qquad [5]$$

Here 2Λ is the physical interface thickness, X_0 is the mole fraction of Mn in the bulk, $X(x)$ is the molar fraction of Mn in the interface, and $E(x)$ is the interaction potential of solute Mn with the austenite/ferrite interface. A wedge-shaped profile is assumed for the Mn-interface interaction potential,[17] as shown in Figure 2. E_0 is the binding energy of Mn, and $2\Delta E$ is the potential difference between ferrite and austenite. It is noted that if E_0 were zero the interaction potential would become a linear interpolation between the chemical potentials in ferrite and austenite.

The concentration profile $X(x)$ of Mn across an interface moving with a velocity of v is given by[17]

$$\frac{\partial}{\partial x}\left(D_{\text{int}} \frac{\partial X(x)}{\partial x} + \frac{D_{\text{int}} X(x)}{RT} \frac{\partial E(x)}{\partial x} + vX(x)\right) = 0, \qquad [6]$$

where D_{int} is the diffusivity of Mn across the austenite/ferrite interface.

As part of the chemical driving pressure, ΔG_{chem}, on the austenite/ferrite interface, Gibbs free energy is dissipated by Mn trans-interface diffusion such that the effective driving pressure for interface migration is

$$\Delta G_{\gamma\alpha} = \Delta G^{\text{chem}} - \Delta G^{\text{dis}}. \qquad [7]$$

III. SIMULATION CONDITION

In the present work, one-dimensional PFM-I, PFM-II, and PFM-III are used to simulate isothermal and cyclic austenite-ferrite transformations in the Fe-0.1C-0.5Mn alloy. First, the isothermal austenite-to-ferrite transformation at 1058.15 K (785 °C) is simulated that occurs prior to the cyclic transformation (see Figure 1(a)). For the cyclic transformation one cycle of the temperature profile shown in Figure 1(a) is employed, *i.e.*, heating from 1058.15 K to 1115.15 K (785 °C to 842 °C) followed by final cooling. Heating and cooling rates are both 10 °C/second. All thermodynamic data are obtained from Thermo-calc® (TCFE6 database), and a linearized phase diagram is used in the phase field models.

D_{int} is assumed to be the geometric average of the bulk diffusivities in ferrite and austenite $D_{\text{int}} = 0.00005 \exp\left(-\frac{247{,}650}{RT}\right)$ m^2/s.[49] The value of the interface mobility is given by $M = 0.058 \exp\left(-\frac{140{,}000}{RT}\right)$ (in mmol/Js) which is obtained from experiments in Fe-C alloys.[50] The binding energy of Mn in PFM-III is taken to be 9.9 kJ/mol.[16] Diffusivities of carbon in austenite and ferrite are assumed to be $D_C^{\gamma} = 0.000015 \exp\left(-\frac{142{,}000}{RT}\right)$ and $D_C^{\alpha} = 0.00022 \exp\left(-\frac{125{,}000}{RT}\right)$ m^2/s, respectively.[40]

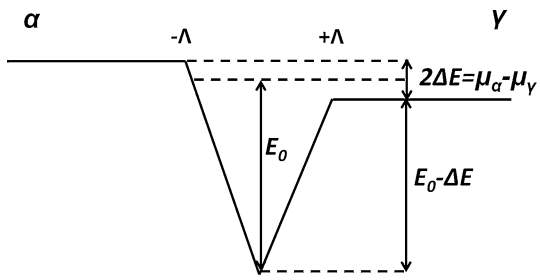

Fig. 2—Schematic of the chemical potential of Mn inside the austenite/ferrite interface with a non-zero binding energy.

The simulation for the isothermal austenite-to-ferrite transformation starts from a mixture of 99.6 pct austenite and 0.4 pct ferrite. The grid spacing is 0.01 μm, and the interface thickness is set to 0.05 μm. The physical thickness 2Λ required in the Gibbs energy dissipation analysis is assumed to be 1 nm. The finite-difference method is used to solve the phase field and diffusion equations in PFM-I and PFM-III. A parallel computer code using OpenMP and message passing interfaces (MPI) was developed and implemented on computer clusters.[51,52] For computational efficiency, PFM-II simulations were conducted using the commercial package MICRESS (MICRostructure Evolution Simulation Software) that also uses the finite-difference method.[53]

IV. RESULTS AND DISCUSSION

A. *Isothermal Austenite-to-Ferrite Transformation*

The isothermal austenite-to-ferrite transformation kinetics at 1058.15 K (785 °C) obtained from the PFM-I, PFM-II, and PFM-III simulations are shown in Figure 3. With PFM-I, both the highest transformation rate and final ferrite fraction are predicted. Taking the role of Mn into account either by Mn portioning (PFM-II) or Gibbs energy dissipation (PFM-III) reduces the transformation rates as well as the final ferrite fraction. The differences in the ferrite fraction after the holding stage at 1058.15 K (785 °C) are, however, comparatively small for the investigated Fe-0.1C-0.5Mn alloy but increase with Mn alloying content as previously shown.[16]

PFM-II is a ternary mixed-mode model and can be used as an example to illustrate mixed-mode transformations in ternary alloys. For this purpose, different values of the interface mobility (0.1M, M, 5M and 10M) have been considered in simulations of the isothermal austenite-to-ferrite transformation at 1058.15 K (785 °C) in the Fe-0.1C-0.5Mn alloy, as illustrated in Figure 4. The value of interface mobility has a considerable influence on the transformation rate but no effect on the final ferrite fraction. The transformation rate increases with the increasing interface mobility until a threshold value (here 5M) has been attained beyond which the transformation rate is essentially independent of interface mobility, *i.e.*, the transformation approaches a purely diffusion controlled growth mode.

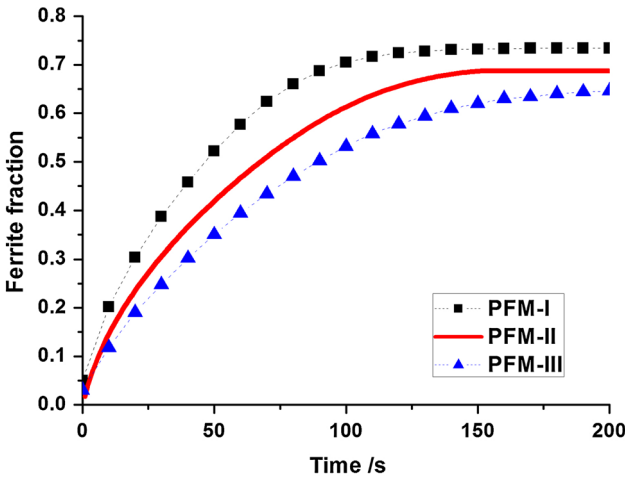

Fig. 3—The simulated fraction of ferrite as a function of time during the isothermal austenite-to-ferrite transformation at 1058.15 K (785 °C) in the Fe-0.1C-0.5Mn alloy.

In Figure 5, the simulated C and Mn profiles are shown for different times during the isothermal austenite-to-ferrite transformation when the value of interface mobility is M. The carbon concentration at the interface deviates significantly from local equilibrium in the initial stage of transformation and is gradually approaching local equilibrium as the transformation proceeds, which is the typical mixed-mode character as previously described by the binary mixed-mode model.[45–47] In the initial stage of the isothermal transformation (t = 10, 20, 30 seconds), there is a very sharp Mn spike (negligible partitioning of Mn) at the interface, and the height of the Mn spike increases as the transformation proceeds. The newly formed ferrite inherits the Mn concentration in austenite, while there is a carbon gradient in austenite, which indicates that long-range diffusion of carbon takes place, *i.e.*, the mixed mode is in this stage a combination of interface reaction and carbon diffusion. At later stages (t = 40 and 50 seconds), Mn starts to redistribute between austenite and ferrite, while the C gradient becomes smaller in austenite, and thus, the transformation rate decreases significantly. The transformation at the later stages becomes increasingly controlled by Mn diffusion, *i.e.*, the mixed-mode regime shifts into a combination of interface reaction with Mn diffusion. Therefore, a transformation mode transition from mixed mode with C diffusion to mixed mode with Mn diffusion takes place during the isothermal austenite-to-ferrite transformation as predicted by the phase field model.

In Figure 6, the simulated profiles of C and Mn are shown during the isothermal austenite-to-ferrite transformation for the value of interface mobility of 0.1M. A comparison between Figures 5 and 6 indicates that the value of the interface mobility has a large effect on both C and Mn diffusion during the austenite-to-ferrite transformation. With the decreasing value of interface mobility, the transformation rate is reduced. As a result, the C gradient in austenite becomes smaller at any given transformation stage, and the C concentration at the interface in austenite decreases. Considering the evolution of the Mn spike, the following observations can be made. For the same transformation time (*e.g.*, 50 seconds), the Mn spike is less pronounced for lower interface mobility as the interface has advanced a smaller distance. For the same fraction transformed (*e.g.*, 50 seconds for M and 250 seconds for 0.1M), however, the Mn spike is much more pronounced for the lower mobility, as the longer transformation time enables increased Mn redistribution.

B. *The Cyclic Phase Transformation*

The simulation results for the cyclic phase transformations in the Fe-0.1C-0.5Mn alloy are shown in

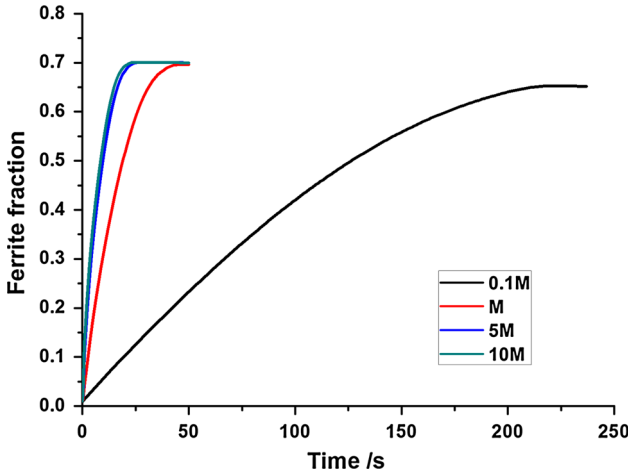

Fig. 4—Isothermal austenite-to-ferrite transformation kinetics at 1058.15 K (785 °C) in the Fe-0.1C-0.5Mn alloy simulated with PFM-II assuming different interface mobilities.

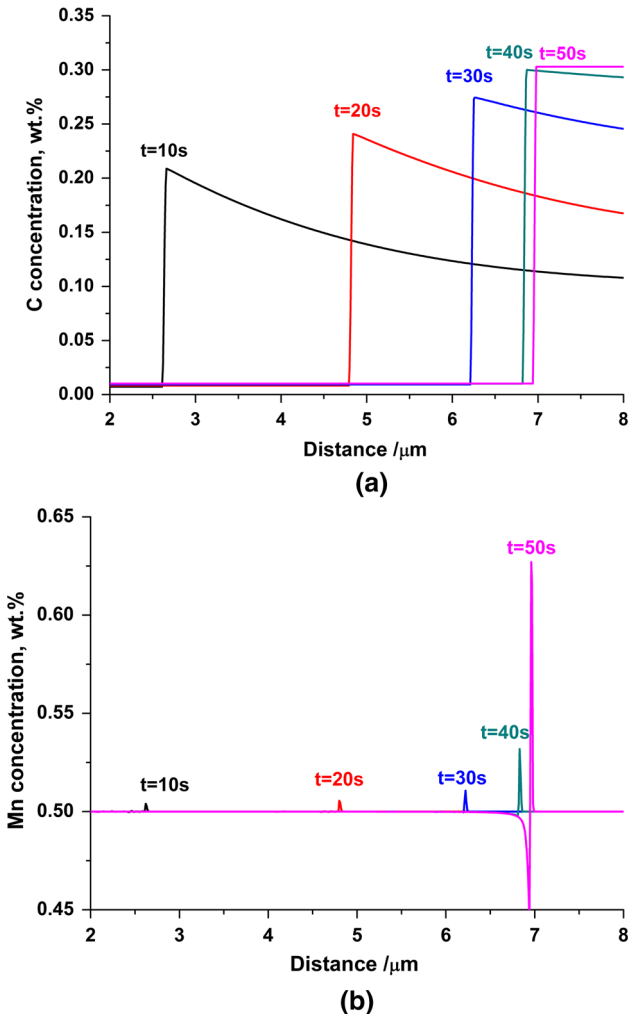

Fig. 5—Simulated C and Mn profiles during the isothermal austenite-to-ferrite transformation at 1058.15 K (785 °C) in the Fe-0.1C-0.5Mn alloy assuming the value of interface mobility as M in PFM-II.

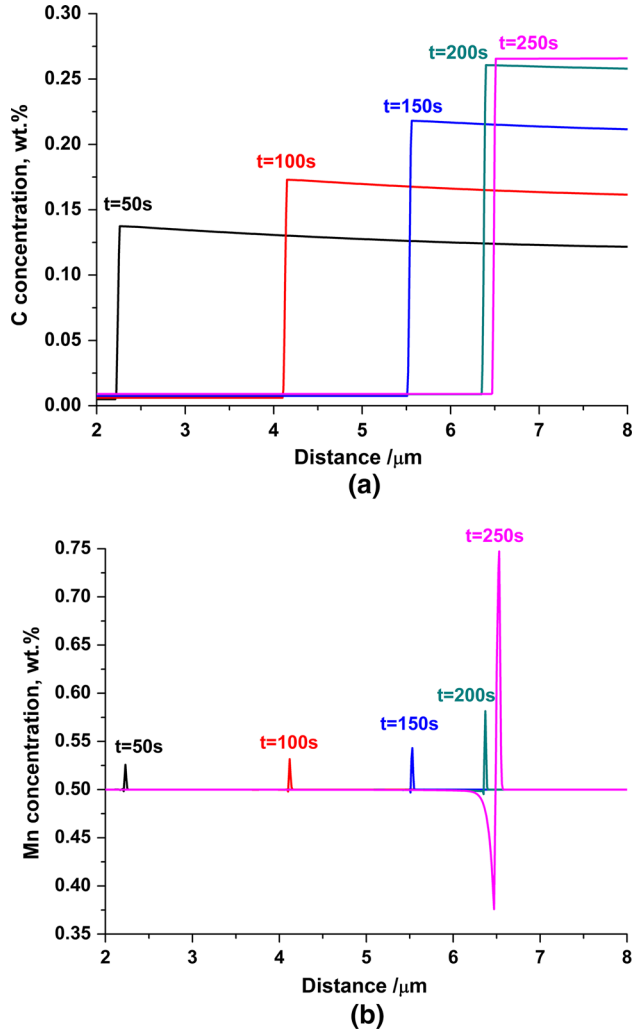

Fig. 6—Simulated C and Mn profiles during the isothermal austenite-to-ferrite transformation at 1058.15 K (785 °C) in the Fe-0.1C-0.5Mn alloy assuming the value of interface mobility as 0.1M in PFM-II.

Figure 7 as obtained by PFM-I, PFM-II, and PFM-III. No stagnant stage and growth retardation are predicted by PFM-I, which does not agree with experiments (Figure 7(a)). PFM-II, on the other hand, can replicate both the stagnant stage and growth retardation phenomenon as observed in the experiments (Figure 7(b)). PFM-III replicates the stagnant stage while the growth retardation phenomenon is not predicted (Figure 7(c)).

The prediction of the stagnant stage and growth retardation by PFM-II can be rationalized by analyzing the evolution of Mn profiles during the cyclic phase transformation. Figure 8 presents the Mn profiles during the heating stage. At the beginning of heating [*e.g.*, 1058.15 K and 1068.15 K (785 °C and 795 °C)], Mn is redistributing between austenite and ferrite with a zig-zag profile, which indicates that the transformation depends on Mn diffusion leading to a very low transformation rate, as indicated in Figure 7(b). When the temperature is increased to 1078.15 K (805 °C), the temperature is sufficiently large such that for the local Mn concentrations at the interface, a driving pressure

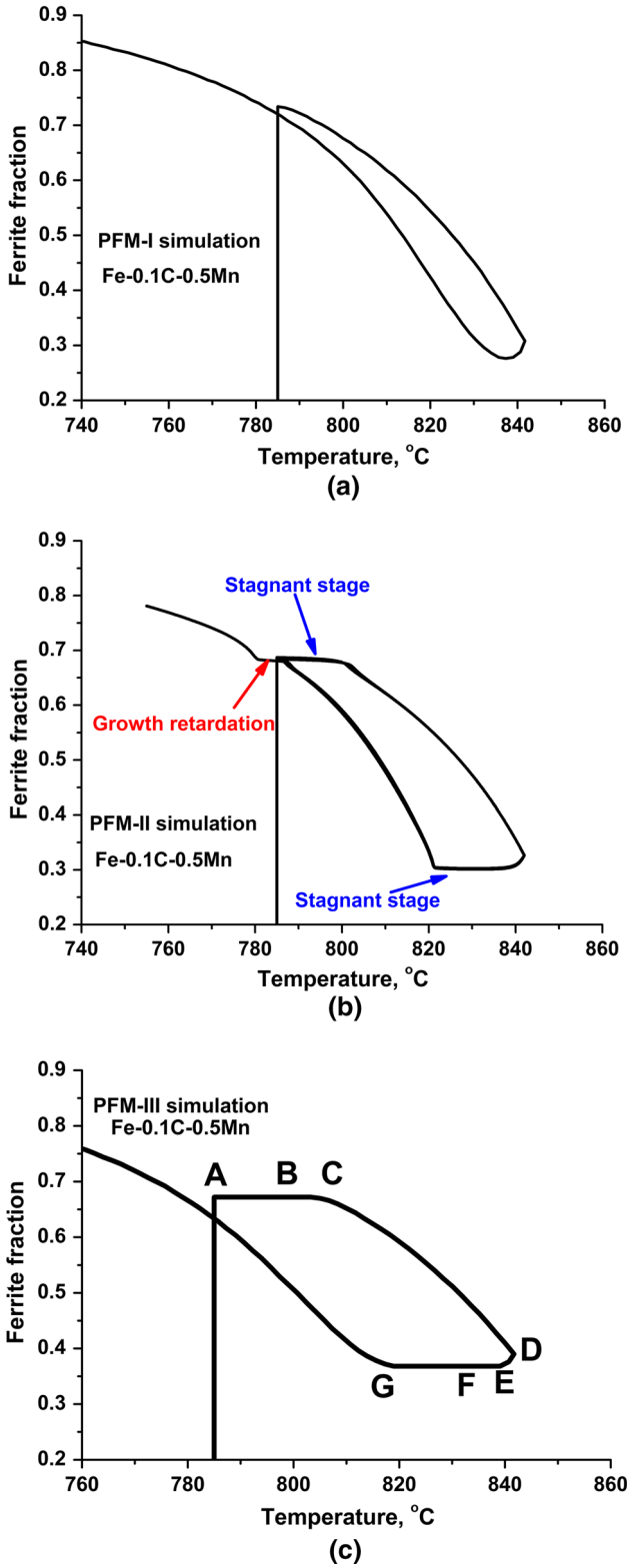

Fig. 7—Ferrite fraction as a function of temperature during the type I (immediate) cyclic phase transformations in the Fe-0.1C-0.5Mn alloy: (*a*) PFM-I simulation; (*b*) PFM-II simulation; (*c*) PFM-III simulation.

exists for austenite formation from ferrite without redistribution of Mn. As a result, the interface starts to migrate at a higher rate and the transformation mode

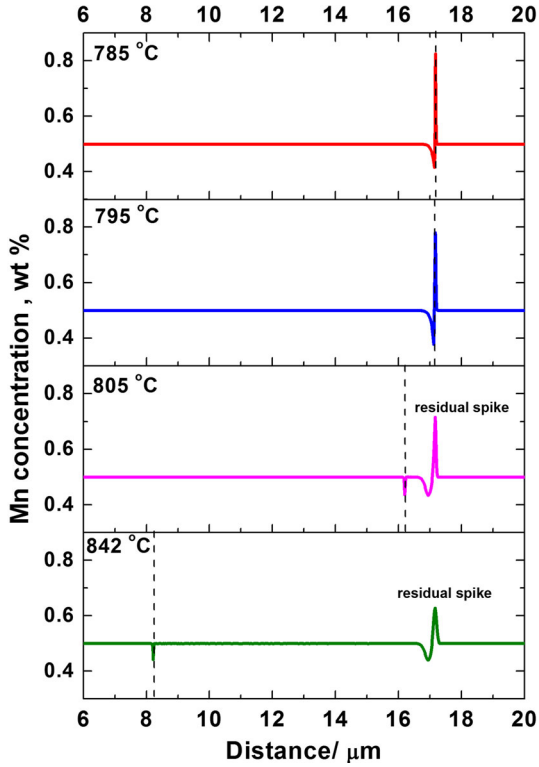

Fig. 8—Mn profiles at different temperatures during the heating stage of the cyclic phase transformation predicted by PFM-II. The dashed black lines indicate the position of the interface. Ferrite and austenite are on the left and right sides of the interface, respectively.

is shifted to mixed mode with carbon diffusion. The interface essentially unpins from the Mn spike that is left behind due to the slow diffusivity of Mn. A sharp negative Mn spike appears at the migrating interface, and the newly formed austenite inherits the nominal Mn concentration. This transformation mode proceeds until the final temperature of the heating cycle, *i.e.*, 1115.15 K (842 °C), is reached. The residual Mn spike left behind the interface is still present albeit with reduced sharpness due to some limited Mn diffusion. The growth mode transition during the heating stage from mixed mode with Mn diffusion to mixed mode with C diffusion leads to the transition from the stagnant stage to the stage with substantial austenite formation.

In Figure 9, the evolution of Mn profiles is shown during the final cooling stage during and after the cyclic phase transformation. At the very beginning of cooling [from 1115.15 K to 1100.15 K (842 °C to 827 °C)], the interface still migrates into ferrite, which leads to the inverse transformation phenomenon as shown Figure 1(b). The local interface concentrations of Mn and C are such that there is still driving pressure remaining for austenite to form even though the temperature is decreased. The inverse transformation stage is characterized by a rather rapid build-up of a Mn spike at the interface indicating a growth mode transition from mixed mode with C diffusion to mixed mode with Mn diffusion, resulting in a stagnant transformation stage. Decreasing the temperature further to 1080.15 K (807 °C), the growth mode changes back

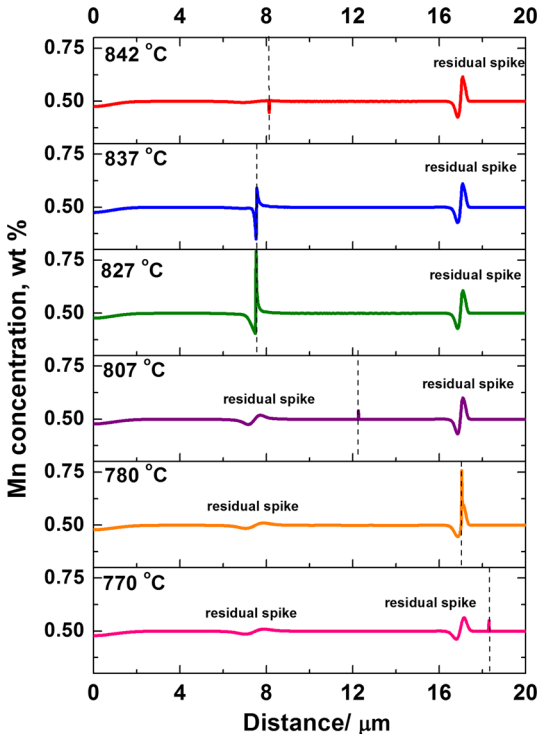

Fig. 9—Mn profiles at different temperatures during the cooling stage of the cyclic phase transformation predicted by PFM-II. The dashed black lines indicate the position of interface. Ferrite and austenite are on the left and right sides of the interface, respectively.

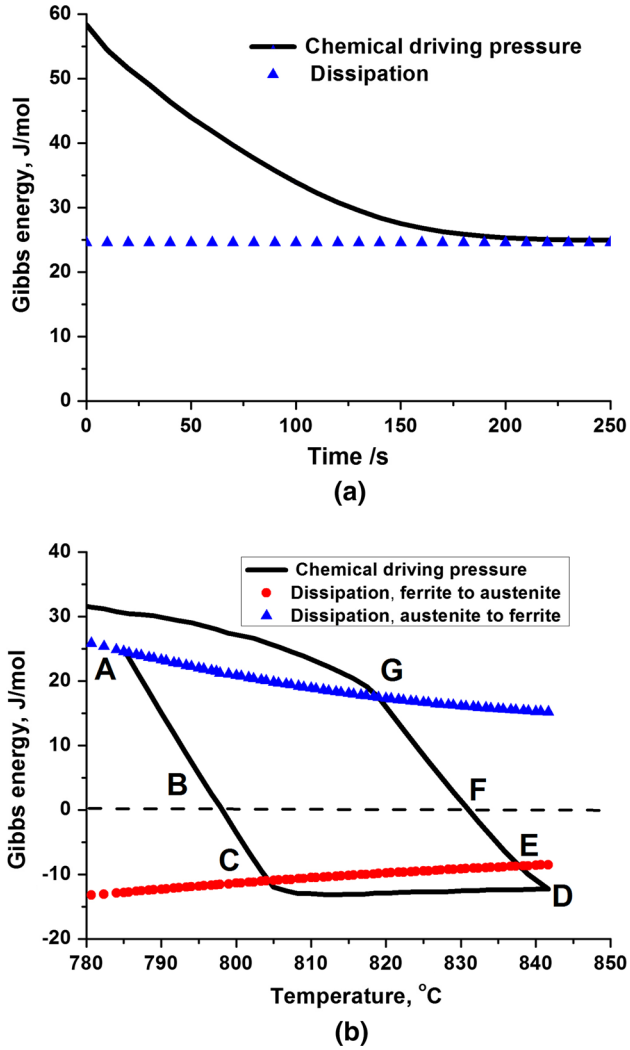

Fig. 10—Chemical driving pressure and dissipation at zero interface velocity in PFM-III: (*a*) during the isothermal austenite-to-ferrite transformation; (*b*) as a function of temperature during the cyclic phase transformation.

into mixed mode with C diffusion, as there is now sufficient driving pressure for ferrite formation to overcome the Mn spike. The interface unpins from the Mn spike that is left behind but disappears comparatively quickly as Mn diffusion in ferrite is substantially larger than in austenite. At the front of the rapidly migrating interface, a sharp Mn spike forms but with small magnitude. At 1053.15 K (780 °C), the migrating interface reaches the residual Mn spike from the heating stage such that a greatly magnified Mn spike forms at the interface. The higher Mn concentration at the austenite side of the interface reduces the driving pressure for ferrite formation that can now only proceed with Mn redistribution, *i.e.*, there is a growth mode transition to mixed mode with Mn diffusion leading to growth retardation even upon further cooling, as shown in Figure 7(b). The chemical driving pressure increases with the decreasing temperature. Once the temperature is sufficiently low [*e.g.*, 1043.15 K (770 °C)], ferrite formation can proceed for the higher Mn concentration by carbon diffusion, *i.e.*, the transformation mode changes back into mixed mode with C diffusion and the interface unpins from the residual Mn spike. Therefore, PFM-II can predict the very complex growth mode transitions between mixed mode with Mn diffusion and mixed mode with C diffusion during the cyclic phase transformation. According to the PFM-II simulations, the stagnant stage is due to mixed-mode growth with Mn diffusion, and the residual Mn spike created by the cyclic phase transformation leads to the growth retardation phenomenon.

To rationalize the prediction of the stagnant stage with PFM-III, it is useful to consider first the evolution of the chemical driving pressure as a function of time during the isothermal austenite-to-ferrite transformation, see Figure 10(a). Here, also the dissipation for zero interface velocity is shown as this provides the limiting driving pressure above which ferrite formation can occur. During the isothermal transformation, the chemical driving pressure decreases due to the increase of C concentration in austenite as the transformation proceeds. When the chemical driving pressure is equal or lower than dissipation for zero velocity, *i.e.*, $\Delta G^{\text{chem}} = \Delta G^{\text{dis}}$, ferrite formation ceases. The same assumption had also been made in the sharp interface model, which can predict the transformation stasis (or incomplete transformation) phenomenon in a series of Fe-C-Mn alloys.[54] Strictly speaking, when

$\Delta G^{chem} = \Delta G^{dis}$, the transformation can only proceed with Mn redistribution that is not considered in PFM-III. As illustrated with PFM-II, the transformation mode with Mn diffusion is very slow such that a zero interface velocity approximation is sufficient for the considered temperature cycles as well as those that are primarily of practical interest during cooling of steel. In the present case, PFM-III predicts that the isothermal austenite-to-ferrite transformation stops at $t = 175$ seconds, as shown in Figure 10(a).

The dissipation at zero velocity and chemical driving pressure are shown as a function of temperature during the cyclic phase transformation in Figure 10(b). The cyclic transformation starts from point A, at which the isothermal transformation has reached the stasis state. The chemical driving pressure decreases with the increasing temperature and reaches zero at point B. In the A–B stage, although there is still chemical driving pressure available for the austenite-to-ferrite transformation, it is lower than dissipation. Therefore, PFM-III predicts that the interface velocity is zero. When the temperature is higher than that at point B, the chemical driving pressure becomes negative, *i.e.*, austenite formation is thermodynamically favored. However, the temperature has to be raised to that of point C before the magnitude of the chemical driving pressure becomes larger than that of dissipation at zero velocity for the ferrite-to-austenite transformation, *i.e.*, the stagnant transformation stage is predicted to continue for the B–C stage. Increasing the temperature above that of point C, the chemical driving pressure for the ferrite-to-austenite transformation is sufficiently large for austenite formation to occur until the maximum temperature of the cycle is reached at point D. The austenite formation stage extends, however, during subsequent cooling until point E even though the magnitude of driving pressure decreases. At point E, the magnitude of driving pressure is equal to that of dissipation and reduces upon further cooling such that a stagnant transformation stage is predicted. Eventually, the temperature is sufficiently low that the driving pressure becomes positive (point F) such that ferrite formation is thermodynamically favored. But the temperature has to be lowered to that of point G before the driving pressure exceeds dissipation. As a result, the stagnant stage predicted by PFM-III extends from E to G during cooling. Cooling below G leads to ferrite formation in PFM-III as the driving pressure is larger than dissipation.

PFM-III using the Gibbs dissipation theory can therefore predict the growth mode transitions during cyclic transformations between mixed mode with C diffusion and stagnant stages which are essentially mixed mode with Mn diffusion in a similar way as the computational more complex PFM-II approach. As long-range diffusion of Mn is not considered in PFM-III, the residual Mn spike in austenite after the cyclic phase transformation cannot be accounted for. Therefore, PFM-III does not predict the growth retardation phenomenon during the final cooling stage.

V. CONCLUSION

Three phase field models (PFM-I, PFM-II, and PFM-III), in which the effect of Mn on the austenite-ferrite interface migration is taken into account by different approaches, have been applied to simulating isothermal and cyclic austenite-ferrite transformations in an Fe-0.1C-1.5Mn alloy. PFM-I, in which only C diffusion is considered while Mn is assumed to be immobile during the phase transformations, can capture neither the stagnant nor the growth retardation stage. Considering both C and Mn diffusion in PFM-II enables the prediction of the stagnant stages during cycling transformations and the subsequent growth retardation phenomenon. In PFM-III, only C diffusion is considered but the Gibbs energy dissipation theory is introduced to account for the effect of Mn on transformation kinetics. PFM-III can replicate the stagnant stages but not growth retardation.

The capabilities of these different PFM approaches have been illustrated in the present work with 1D simulations. From a more rigorous perspective, it is important to predict the microstructures resulting from the austenite-ferrite transformations with 3D or at least 2D simulations. The high computational costs of PFM-II that considers long-range diffusion of two species with orders of magnitude different diffusion rates limit its applicability to these more demanding simulations. Thus, PFM-III may be an attractive alternative for simulation of microstructure evolution as it can describe without considering long-range diffusion of Mn general effects of Mn on the austenite-ferrite interface migration for both ferrite and austenite formation. PFM-III is, however, limited to heat treatment scenarios where Mn redistribution can be neglected. To accurately account for cases with Mn diffusion, it is suggested to combine PFM-II and PFM-III, *i.e.*, to consider both long-range Mn diffusion as well as dissipation due to interfacial Mn diffusion. Interfacial segregation of Mn is indeed a relevant phenomenon that has been inferred from both experimental and theoretical studies.[5,55]

REFERENCES

1. M. Hillert: The growth of ferrite, bainite and martensite. Internal report, Royal Institute of Technology, 1960.
2. H.I. Aaronson, M. Enomoto, and J.K. Lee: *Mechanisms of Diffusional Phase Transformations in Metals and Alloys*, Taylor & Francis Group, New York, 2010.
3. E. Pereloma and D. Edmonds: *Phase Transformation in Steels*, Woodhead Publishing, Cambridge, 2012.
4. G. Purdy, J. Ågren, A. Borgenstam, Y. Bréchet, M. Enomoto, T. Furuhara, E. Gamsjäger, M. Gouné, M. Hillert, C. Hutchinson, M. Militzer, and H. Zurob: *Metall. Mater. Trans. A*, 2011, vol. 42A, pp. 3703–18.
5. M. Gouné, F. Danoix, J. Ågren, Y. Bréchet, C. Hutchinson, M. Militzer, G. Purdy, S. van der Zwaag, and H. Zurob: *Mater. Sci. Eng. R*, 2015, vol. 92, pp. 1–38.
6. M. Hillert: Introduction to paraequilibrium, Internal report, Swedish Institute of Metals Research, Stockholm, 1953.
7. A. Hultgren: *Trans. ASM.*, 1947, vol. 39, pp. 915–1005.
8. C. Zener: *J. Appl. Phys.*, 1949, vol. 20, pp. 950–53.
9. J.S. Kirkaldy: *Can. J. Phys.*, 1958, vol. 36, pp. 907–16.
10. D.E. Coates: *Metall. Trans.*, 1972, vol. 3, pp. 1203–12.

11. G.R. Purdy and Y. Bréchet: *Acta Metall.*, 1995, vol. 43, pp. 3763–74.
12. M. Enomoto: *Acta Mater.*, 1999, vol. 47, pp. 3533–40.
13. J. Odqvist, M. Hillert, and J. Ågren: *Acta Mater.*, 2002, vol. 50, pp. 3211–25.
14. H. Zurob, D. Panahi, C. Hutchinson, Y. Bréchet, and G. Purdy: *Metall. Mater. Trans. A*, 2013, vol. 44A, pp. 3456–71.
15. H. Chen, A. Borgenstam, J. Odqvist, I. Zuazo, J. Ågren, and S. van der Zwaag: *Acta Mater.*, 2013, vol. 61, pp. 4512–23.
16. H. Chen and S. van der Zwaag: *Acta Mater*, 2014, vol. 72, pp. 1–12.
17. J.W. Cahn: *Acta Metall.*, 1962, vol. 10, pp. 789–98.
18. M. Hillert and B. Sundman: *Acta Metall.*, 1976, vol. 24, pp. 731–43.
19. M. Hillert, J. Odqvist, and J. Ågren: *Scripta Mater.*, 2001, vol. 45, pp. 221–27.
20. M. Hillert: *Acta Mater.*, 2004, vol. 52, pp. 5289–93.
21. K. Oi, C. Lux, and G.R. Purdy: *Acta Mater.*, 2000, vol. 48, pp. 2147–55.
22. Z.D. Li, Z.G. Yang, C. Zhang, and Z.Q. Liu: *Mater. Sci. Eng. A*, 2010, vol. 527, pp. 4406–11.
23. H. Chen, W. Xu, G. Mohamed, and S. van der Zwaag: *Philos. Magn. Lett.*, 2012, vol. 92, pp. 547–55.
24. Z.Q. Liu, G. Miyamoto, Z.G. Yang, and T. Furuhara: *Acta Mater.*, 2013, vol. 61, pp. 3120–29.
25. A. Beche, H.S. Zurob, and C.R. Hutchinson: *Mater. Trans. A*, 2007, vol. 38A, pp. 2950–55.
26. H.S. Zurob, C.R. Hutchinson, A. Beche, G.R. Purdy, and Y. Bréchet: *Acta Mater.*, 2008, vol. 56, pp. 2203–11.
27. H.S. Zurob, C.R. Hutchinson, Y. Bréchet, H. Seyedrezai, and G.R. Purdy: *Acta Mater.*, 2009, vol. 57, pp. 2781–92.
28. C.R. Hutchinson, A. Fuchsmann, H.S. Zurob, and Y. Bréchet: *Scripta Mater.*, 2004, vol. 50, pp. 285–89.
29. H. Chen and S. van der Zwaag: *Comput. Mater. Sci.*, 2010, vol. 49, pp. 801–13.
30. H. Chen, M. Gouné, and S. van der Zwaag: *Comput. Mater. Sci.*, 2012, vol. 55, pp. 34–43.
31. H. Chen, R. Kuziak, and S. van der Zwaag: *Metall. Mater. Trans. A*, 2013, vol. 44A, pp. 5617–21.
32. H. Chen and S. van der Zwaag: *Acta Mater.*, 2013, vol. 61, pp. 1338–49.
33. H. Chen, E. Gamsjäger, S. Schider, and S. van der Zwaag: *Acta Mater.*, 2013, vol. 61, pp. 2414–24.
34. H. Chen, B. Appolaire, and S. van der Zwaag: *Acta Mater.*, 2011, vol. 59, pp. 6751–60.
35. E. Gamsjäger, H. Chen, and S. van der Zwaag: *Comput. Mater. Sci.*, 2014, vol. 83, pp. 92–100.
36. C.J. Huang, D.J. Browne, and S. McFadden: *Acta Mater.*, 2006, vol. 54, pp. 11–21.
37. M.G. Mecozzi, J. Sietsma, S. van Der Zwaag, M. Apel, P. Schaffnit, and I. Steinbach: *Metall. Mater. Trans. A*, 2005, vol. 36A, pp. 2327–40.
38. M.G. Mecozzi, M. Militzer, J. Sietsma, and S. van der Zwaag: *Metall. Mater. Trans. A*, 2008, vol. 39A, pp. 1237–47.
39. M.G. Mecozzi, J. Sietsma, and S. van der Zwaag: *Acta Mater.*, 2006, vol. 54, pp. 1431–40.
40. M. Militzer: *Curr. Opin. Solid State Mater. Sci.*, 2011, vol. 15, pp. 106–15.
41. M. Militzer, M.G. Mecozzi, J. Sietsma, and S. van der Zwaag: *Acta Mater.*, 2006, vol. 54, pp. 3961–72.
42. I. Steinbach and F. Pezzolla: *Phys. Nonlinear Phenom.*, 1999, vol. 134, pp. 385–93.
43. J. Eiken, B. Böttger, and I. Steinbach: *Phys. Rev. E*, 2006, vol. 73, p. 6.
44. M. Mecozzi, J. Eiken, M. Apel, and J. Sietsma: *Comput. Mater. Sci.*, 2011, vol. 50, pp. 1846–53.
45. J. Sietsma and S. van der Zwaag: *Acta Mater.*, 2004, vol. 52, pp. 4143–52.
46. H. Chen and S. van der Zwaag: *J. Mater. Sci.*, 2011, vol. 46, pp. 1328–36.
47. Z. Liu, Z.G. Yang, Z. Li, Z. Liu, and C. Zhang: *Acta Metall. Sin.*, 2010, vol. 46, pp. 390–95.
48. H. Chen, Y.C. Liu, Z.S. Yan, Y.L. Li, and L.F. Zhang: *Appl. Phys. A*, 2010, vol. 98, pp. 211–17.
49. B. Zhu, H. Chen, and M. Militzer: *Comput. Mater. Sci.*, 2015, vol. 108, pp. 333–41.
50. G.P. Krielaart, J. Sietsma, and S. van der Zwaag: *Mater. Sci. Eng. A*, 1997, vol. 237, pp. 216–23.
51. B. Zhu and M. Militzer: *Model. Simul. Mater. Sci. Eng.*, 2012, vol. 20, p. 085011.
52. B. Zhu and M. Militzer: *Metall. Mater. Trans. A*, 2015, vol. 46A, pp. 1073–84.
53. MICRESS, Software developed in ACCESS is an independent research center associated with the Technical University of Aachen.
54. H. Chen, K. Zhu, L. Zhao, and S. van der Zwaag: *Acta Mater.*, 2013, vol. 61, pp. 5458–68.
55. H. Jin, I. Elfimov, and M. Militzer: *J. Appl. Phys.*, 2014, vol. 115, p. 093506.